Chapter 13
Uncertainty Effects on Bike Spoke Wheel Modal Behaviour

E. Bonisoli, A. D. Vella, and S. Venturini

Abstract In bicycles, one of the components which mostly influences the global system dynamics is the wheel-tyre subsystem. In this paper, the modal behaviour of a bike spoke wheel is numerically and experimentally investigated focusing on the characterisation of the spoke pretension effect, role of boundary conditions and parameter uncertainties.

A linearised parametric finite element model (FEM) is developed with the open-source code LUPOS in Matlab® environment. A detailed description of the model which includes several components, i.e. rim, hub, spokes and hub gears, is given. The FEM model is based on a reduced set of key nodes belonging to the wheel cross section profile, material and geometrical characteristic assignment and automated meshing procedure, allowing reduced computational effort and high model accuracy.

Experimental modal analysis is conducted on the wheel, and critical issues in the pole identification are highlighted, due to the high modal density given by the spokes and uncertainties. A further numerical investigation based on a variational approach is applied to investigate the role of system uncertainties on the modal parameters. The analysis shows that the identification issues are mainly related to spoke pretension, cross contact and boundary conditions. Moreover, the spoke pretension uncertainty induces a mistuning in the structure and the corresponding loss of axial symmetry. The fine model updating of the preliminary model is then achieved optimising geometrical and material properties of the components as well spoke pretension.

Keywords Parametric modal analysis · Uncertainty quantification · Boundary conditions · Model updating · Stress stiffening

13.1 Introduction

In wheeled vehicle applications, the wheel subsystem acts as support for the tyre and is directly or indirectly (by means of a suspension system) connected to the vehicle chassis. The interactions between the road surface and the tyre thread, which can be distinguished into impacts and adhesion mechanisms, produce radial and tangential vibrations [1]. These phenomena constitute the main noise source over 40 km/h in passenger car and 60 km/h in trucks [2]. It can be taken for granted that the wheel subsystem represents also a relevant part in the vibration transmission chain, from the ground irregularities to the vehicle passengers [3].

Since tyre and wheel are strictly correlated to vibration and acoustic ride comfort, the state-of-the-art extensively investigates tyre and tyre-wheel assembly modal behaviour, from both experimental and numerical point of view. In [4, 5] the effect of the angular velocity, vertical load and air pressure on the tyre dynamics was studied. Doria et al. [6] identified the first five out-of-plane mode shapes of motorcycle tyres to estimate the relaxation length. FTYRE model was discussed in [7]. Pinnington et al. [8] showed that tyre belt can be considered rigid in tangential direction above 500 Hz. The first air cavity resonance in the unloaded configuration occurs between 200 Hz and 250 Hz [9]. It was experimentally proved that interior noise below than 400 Hz is related to forces at the spindle [7]. In automotive field, frequency ranges to evaluate whole-body and hand-transmitted vibration discomfort are, respectively, up to 80 Hz and 1000 Hz [10].

E. Bonisoli (✉) · A. D. Vella · S. Venturini
Department of Mechanical and Aerospace Engineering, Politecnico di Torino, Torino, Italy
e-mail: elvio.bonisoli@polito.it; angelo.vella@polito.it; simone.venturini@polito.it

Z. Mao (eds.), *Model Validation and Uncertainty Quantification, Volume 3*, Conference Proceedings of the Society for Experimental Mechanics Series, https://doi.org/10.1007/978-3-031-04090-0_13

Several analytical and FEM models were developed in order to study specific frequency ranges and tyre phenomena. Flexible ring with an elastic foundation can describe in-plane dynamics but not the cross-sectional dynamics. Flat model is used to describe road deformation and phenomena higher than 400 Hz.

If on one hand the tyre was deeply discussed, on the other hand, a limited amount of available data deals more closely to the wheel subsystem, both in automotive and in other applications. In order to validate a simplified tyre model to predict structure-borne interior noise, Kindt et al. [1] showed the first four natural frequencies identified on 205/55 R16 steel wheel in the clamped configuration: the axial mode occurs at 393.2 Hz while the first and the second bending mode shapes, respectively, at 167.5 Hz and 440.7 Hz. Steel wheel is a relatively simple system to study since it is constituted by a disc mated to a rim by interference fit. In [11] the authors discussed a novel non-destructive method to evaluate the fitting force starting from stiffening effect and experimental data.

On the other side, the bike spoke wheel which is discussed in this work is an example of complex subsystem to investigate because of its several potential uncertainties. The case study deals with the analysis of the modal behaviour of a bike spoke wheel, focusing on structure uncertainties and stiffening effect due to spoke preload. The presence of the spokes undoubtedly plays the key role since each of them is clamped with a certain axial preload on the rim, tangentially pulled through the rim holes and then again clamped on the rim. Moreover, the spokes are in contact with each other. The nominal preload may also decrease in a different amount after a certain working period. Spoke contacts, different levels of preload and peculiar boundaries together with geometrical and material properties of the rim and the hub make the bike spoke wheel a challenging case to study and to model. To do so, model updating (MU) techniques can be exploited.

Eigenvalue sensitivity to parameters uncertainties was used in [12, 13] to evaluate the stress-stiffening effect in aluminium frame. MU techniques can be also based on optimisation problems: for instance, in [14–16], the target was the evaluation of residual stress from dynamic measurements. An alternative to take advantage from eigenvalue sensitivity to uncertainties is represented by the methodology proposed by Bahra and Greening [17] which monitored the Modal Assurance Criterion (MAC) [18, 19]. The variability in dynamic behaviour due to constraint uncertainties [20] is a well-known issue in industrial field. In automotive manufacturing, frequency response function (FRF) variability is usually considered. In [21–24] geometrical and material uncertainties were introduced in FEM models to reproduce the FRF variability experienced in the experimental analysis. In this case study, a minimisation problem is solved varying uncertain parameters to tune the FEM model in terms of natural frequency similarity. The mode tracking is performed with MAC.

The paper is organised as follows:

In Sect. 13.1 the required theoretical background and the case study are defined.
Sect. 13.2 deals with the modelling phase with a specific focus on the assumption made and implementation in LUPOS [25] software.
In Sect. 13.3 the experimental modal analysis (EMA) on the wheel is described. Results and numerical-experimental comparison are shown.
In Sect. 13.4 the optimisation problem to achieve the FEM model tuning is discussed and results are presented.

13.2 Model Updating by Mode Shape Tracing

The proposed method aims at efficiently characterising the effect of uncertainties on the dynamics of a mechanical component. The uncertainties in the geometrical and material properties are exploited to tune the finite element (FE) model: the component pre-stress induced in the structure during the assembly phase is also considered.

The starting point of the presented approach is the modal analysis of the full assembly. Modal analysis is nowadays a robust and diffused technique to perform dynamic behaviour prediction both exploiting finite elements analysis (FEA) with commercial software and laboratory testing with experimental modal analysis (EMA).

Once the modal properties of the assembly are known, the tuning is performed by design to modal analysis (DMA) approach [26–28] exploiting the influence of uncertain parameter variability on the global structural mode shapes. The fine model updating is automatically performed by the optimisation problem based on the aforementioned method. The DMA approach was introduced for investigation, re-design and improvement purposes by exploiting the Modal Assurance Criterion (MAC) introduced by Allemang in 1982 [18]; in summary, it consisted in an index defined in the $[0 \div 1]$ interval computed between mode shapes j and k whose value is as higher as the two mode shapes are identical based on the original index; the MACW2 correlation index is adopted to include eigenvalue contribution (gap or proximity) in the mode shape correlation

assessment. This index is the instrument to distinguish similar mode shapes with spaced natural frequencies. Equation 13.1 represents the MACW2 between eigenvectors φ_j and φ_k, where ω_j^2 and ω_k^2 are the related eigenvalues:

$$MACW2_{j,k} = \frac{\left[\boldsymbol{\varphi}_j^T \ \boldsymbol{\varphi}_k\right]^2}{\left[\boldsymbol{\varphi}_j^T \ \boldsymbol{\varphi}_j\right]\left[\boldsymbol{\varphi}_k^T \ \boldsymbol{\varphi}_k\right]} e^{-\sqrt{2\left|\frac{\omega_j^2-\omega_k^2}{\omega_j^2+\omega_k^2}\right|}} \tag{13.1}$$

Starting from consistent experience in optimisation processes for MU, gradient-based Matlab tool *fmincon* [29] is used in the methodology. The optimisation is performed by following the reported steps:

- Preliminary analysis on the model to estimate expected nominal properties and parameter sensitivity.
- Optimisation run with initial optimising parameters slightly shifted from nominal condition.

The objective function is developed as a composition of the error in terms of MACW2 and the discrepancy on the model weight as shown in Eq. 13.2:

$$\begin{aligned} \text{ObjFnc} &= \text{RE}\,(\text{MACW2}) + \text{RE}(m) \\ \text{RE}\,(\text{MACW2}) &= \frac{n - \sum_{r=1}^{n} \max\left(\text{MACW2}_{r,k} | \forall \ k\right)}{n} \\ \text{RE}(m) &= \frac{\left|m_{ref} - m\right|}{m_{ref}} \end{aligned} \tag{13.2}$$

where:

- n are the number of experimental modes considered in the updating
- m_{ref} is the reference mass of the structure
- m is the mass of the updating structure.

The objective function solution is defined in $[0 \div 2]$ interval and has to be minimised. The weights of eigenvectors and eigenvalues are identical and collected in the MACW2 term (see Eq. 13.1), while the relative error on the mass guarantees that the properties are not changed without physical meaning.

13.3 Rear Bike Spoke Wheel in Free-Free Conditions

In this section, the development of the preliminary FE model of a rear bike spoke wheel is discussed. The system under analysis is a prestressed structure in which the spoke preload is imposed during the assembly procedure. The wheel can be theoretically considered as an axisymmetric structure composed by several components. In the bike wheel, typically the hub is linked to the rim by a set of spokes which are tensioned by acting on nipples, i.e. rivets located in the rim. In this case study, transmission gears are also included. Depending on the type of wheel, spoke pretension can be modified directly acting on the nipples. The wheel under analysis is based on the rim Rigida X-PLORER Safety Line 26″ 559–19 with 36 spoke holes [30] in aluminium material. The wheel involves a Shimano HB-TS30 hub in aluminium. The spokes are made of steel and consist of rod elements whose diameter is equal to 2 mm: their purpose is linking the hub to the rim. The maximum allowable pretension of the spokes is equal to 1300 N [30]. The spokes pattern is usually classified by the number of in-plane intersections between the spokes. In this case study, the pattern is classified as a "3X" [31] which is based on a 4spokes connection between the rim and the inner and outer hub flanges. This configuration involves spoke contact.

In Fig. 13.1 it is shown the resulting developed preliminary FE model.

The FE model is developed in LUPOS open source FE code in Matlab. The model is parametrically built by revolution of a cross-sectional pattern of nodes and then assigning material and geometry properties to the two main subsystem, i.e. the rim and the hub. On the contrary, the spokes are procedurally introduced in the FE model by imposing the "3X" pattern [31]. Spoke contact spots are automatically identified by the code, and spherical joints are introduced between the interface nodes supposing the contact as a constraint. The hub and the rim are described with 4-node shell element with constant thickness while the spokes with 1D Euler-Bernoulli rod elements and the gears as 1D elements. The model stands a total of 2146

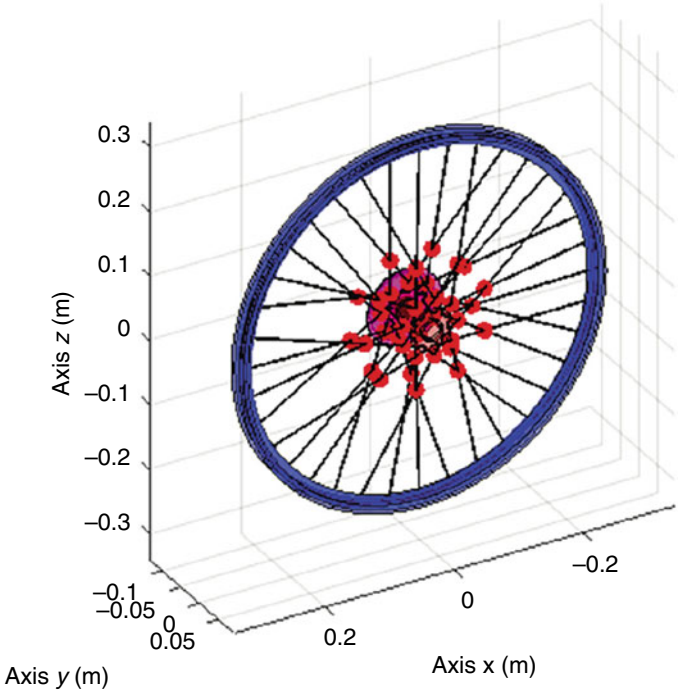

Fig. 13.1 FE model

Table 13.1 Geometrical and material properties

Component	Parameter	Value
Rim	E, Young Modulus [GPa]	70
	ρ, density [kg/m^3]	2700
	t, thickness [mm]	0.8–2.0
Hub	E, Young Modulus [GPa]	70
	ρ, density [kg/m^3]	2700
	t, thickness [mm]	3–8
Spokes	E, Young Modulus [GPa]	210
	ρ, density [kg/m^3]	7800
	$\varnothing$, diameter [mm]	2
	N, pretension [N]	1200
Gear	E, Young Modulus [GPa]	210
	ρ, density [kg/m^3]	7800

nodes, with 1036 1D elements and 1440 2D elements for a total amount of 12876 degrees of freedom in free-free conditions. The mass of the starting model is 1.5253 kg, while 1.5774 kg is the mass of the real assembly.

In Table 13.1, the main geometrical and material data are reported.

MoGeSeC methodology [32] is applied to the starting model in order to define the master nodes for roving hammer EMA. In total, four PCB 356A15 tri-axial accelerometers whose masses are equal to 14.2 g are placed on the wheel, three distributed on the rim flanges and one on the hub. 50 hammer locations are identified, and 48 nodes are circumferentially located at angular positions multiple of $\pi/2$, $\pi/4$, $\pi/6$ for the axial and radial response, while 2 nodes are located on the outer hub flange for the axial response only. In Fig. 13.2, the sensor locations and the hammered points are sketched.

13.3.1 Effect of Spoke Pretension

The spoke tension could be operatively defined during the mounting procedure of the bike wheel. Nevertheless, the preload of the bike wheel under analysis is considered an unknown parameter since it is not possible to regulate or easily measure. From a preliminary study of the modal behaviour of the system, a high density of modes related to spokes local dynamics is

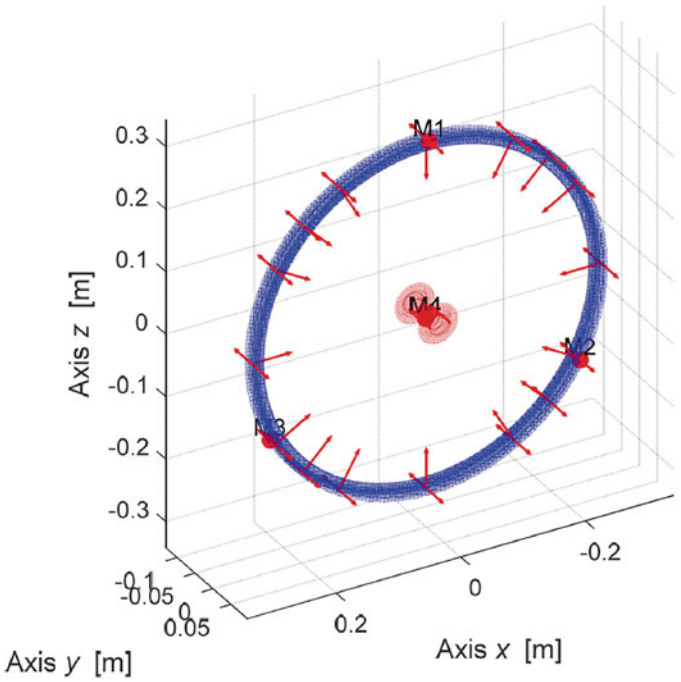

Fig. 13.2 Accelerometers and hammered locations

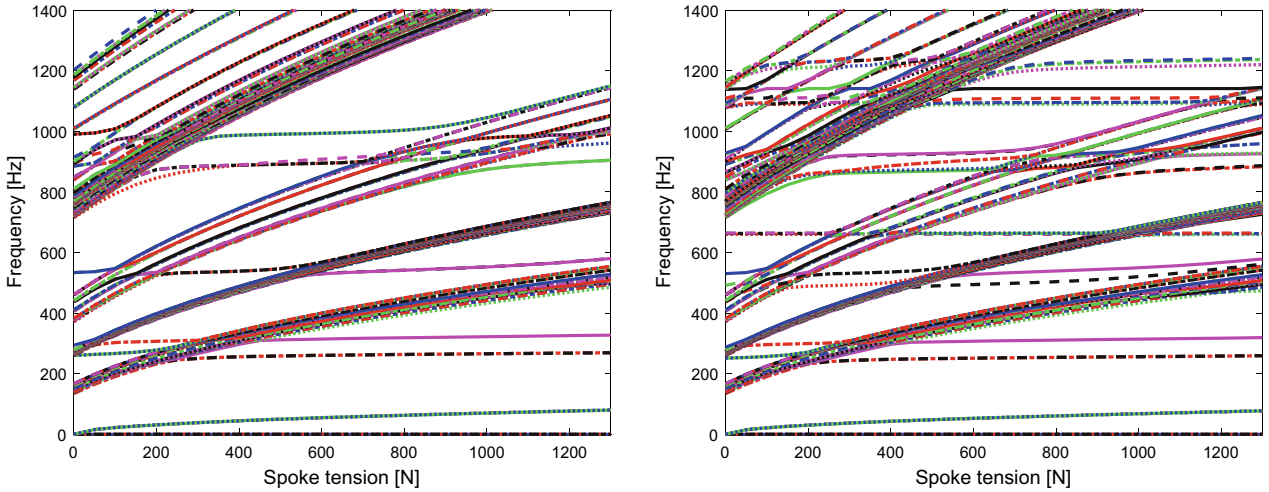

Fig. 13.3 Parametric real modal analysis, first 200 modes: without accelerometers (left) and with accelerometers (right)

expected. This property is mainly caused by the high difference in thickness between spokes and the rim. A parametric real modal analysis is performed on the FE model assuming the same tension on all the spokes. The first 200 natural frequencies are identified by varying the spoke tension T = [0: 50: 1200] N.

In Fig. 13.3, on the left, the aforementioned density of mode shapes is already emphasised: applying spoke pretension equal to 0 N, the first 100 modes occur in the first 600 Hz, and it is very challenging to distinguish local spoke modes and structure modes. Moreover, it is possible to identify subsets of modes which are strongly affected by the pretension and monotonically increasing in frequency: these modes are related to spoke local dynamics. On the other hand, single mode shapes or couples of mode shapes, not so influenced by the pretension, can be associated with the rim and the hub dynamics. Multiplicity equal to 2 of some mode shapes is due to the pseudo-axisymmetric. In the experimental campaign, the introduction of accelerometers makes the structure no more axisymmetric: some of the coupled eigenvalues are spaced, while some couple of eigenvectors are split in more than two mode shapes on a certain frequency range.

Figure 13.3, on the right, shows how the density increases following the first 200 modes: the addition of accelerometers is almost marginal on the structure, while the hardest difficulty in correlating the model to experimental results will be caused by correct estimation of the spoke tension which couples spoke and wheel modes.

13.3.2 Experimental Modal Analysis

In this subparagraph, the experimental setup, the mode shapes and the natural frequencies coming from the numerical and the experimental results are reported.

In the experimental campaign, the bike wheel is hanged by an elastic rubber band to a pneumatic crane, to perform roving hammer EMA in free-free conditions. The rubber band is passed through the hollow shaft of the wheel. The folded rubber band under static deformation induced by the bike wheel weight has a vertical length of 0.61 m. The wheel does not enter in contact with the rubber band during the entire measuring activity. As previously mentioned, four tri-axial accelerometers PCB 356A15 are placed in the identified master node locations using MoGeSeC technique. The impact hammer PCB 086C03 is used to excite the structure. All 40 locations are hammered on the wheel. The locations are radially distributed every 30 ° and 45 ° to describe 2-lobe and 3-lobe mode shapes at best and 4-lobe ones with compromises. The radial locations on the rim follow the rim features, deviating from nipple hole locations (Fig. 13.4).

Siemens LMS SCADAS Mobile was used to acquire and post-process the hammer and accelerometer signals. The EMA is performed in bandwidth 0÷4096 Hz with an acquisition time of 1 s (frequency resolution of 1 Hz) and linear average measure of five repetitions; the force-exponential window is used for the hammer input signal over 0.6% of samples, while an exponential window with a decay of 30% is applied to accelerometer output signal. H1 is used as FRF estimator. The identification is performed in the bandwidth 0÷2000 Hz.

In Fig. 13.5 the sum of all the FRFs is reported in red line. Black dot-dot lines represent the identified 19 poles.

Since the pole identification was hard to achieve, the frequency range is divided in 400 Hz intervals, then the identified subsets of poles are grouped. The main structure mode shapes, in correspondence of the higher peaks, are evident. At the same time, except for the first couple of mode shapes (at almost 190 Hz) and the first single mode shape (at almost 230 Hz), the amplitude curve is highly rugged: minor peaks in correspondence of structural mode shapes are due to the presence of the same mode shapes, sometimes mixed each other, many times because of the asymmetries caused by unbalanced masses and different spoke pretensions. Other peaks are probably due to local spoke mode shapes and cannot be identified.

Fig. 13.4 Experimental setup

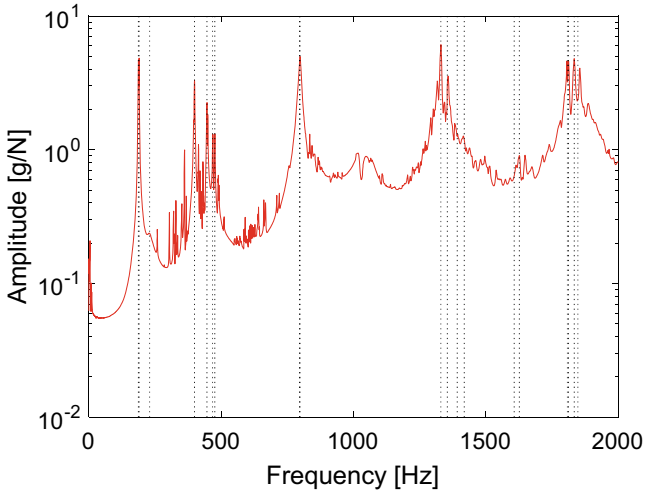

Fig. 13.5 Sum of all the experimental FRFs

13.3.3 Numerical to Experimental Comparison

In this subparagraph, the comparison between the experimental and the numerical results is carried out. The comparison is carried out considering the FE primary model and only the subset of degrees of freedom (DOFs) experimentally used for forcing or measuring the hammer response. Figure 13.6 represents the MAC computed between the experimental mode shapes (along *y*-axis) and the first 214 numerical mode shapes (along *x*-axis). The rigid body motions are deleted from both the numerical and the experimental mode shape sets.

As highlighted by Fig. 13.6, some experimental mode shapes are well-correlated to more than one numerical mode shape: this phenomenon is due to the fact that all the local spoke mode shapes involve a small rim deformation which can be more or less similar to other structural mode shapes. It was not possible to monitor spoke response during the experimental activity to isolate this issue. As mentioned in Sect. 13.2, the identification is also performed using MACW2 index to track mode shapes in function of the corresponding eigenvalue.

Figure 13.7 represents MAC index (experimental along *y*-axis, numerical along *x*-axis) between all the identified experimental mode shapes and the most interesting numerical mode shapes in function of the relative natural frequencies.

The dash-dot black line represents the iso-frequency line on which occurs the perfect similarity between EMA and FEA results. As it is clear, the preliminary FE model can catch the principal mode shapes experimentally identified, but it tends to overestimate the frequencies. The model seems to be more rigid than the real bike wheel.

Now some details are given on the identification of the 19 experimental structural mode shapes related to the modal deformation of the whole rim and the axial displacement of the hub. The first three mode shapes refer to the 1st bending and the axial mode shape. Secondly, there is a group of four identified mode shapes which refer to the 2nd bending. Then there is a couple of mode shapes around 800 Hz which represents the 3rd bending. Then there are four mode shapes from 1330 Hz to 1420 Hz which are the 4th bending and the in-plane 2-lobe mode shapes. At almost 1600 Hz the in-plane 3-lobe mode shapes are detected. Finally, there are four peaks representing the 5th bending. The 4-lobe in-plane mode shapes are not experimentally found, probably because of the frequency bandwidth. In Fig. 13.7, very good correlation can be remarked for the 1st and the 2nd bending mode shapes (higher than 90%) as well as for the axial mode shape (97%). A bit smaller MAC correspond to the 2nd and the 4th bending mode shapes, respectively higher than 75% and 62%. The 2-lobe in-plane mode shapes own a poor correlation, almost 25%, while the MAC increases in the 3-lobe case. Even the 5th bending mode shapes are well correlated.

In Table 13.2, an overview of the numerical and the experimental frequencies is proposed. In the second and in the third columns, natural frequencies numerically achieved with and without the mass addition due to accelerometer are reported, while in the fourth column the experimental frequencies of the identified mode shapes are shown.

From the numerical-experimental comparison shown in this section, a very high modal density is achieved performing the modal analysis of the model due to the presence of the several rods with different pretensions. The defined hammering locations allow to mainly identify bending mode shapes, and the proposed MACW2 approach is suitable for correlation when

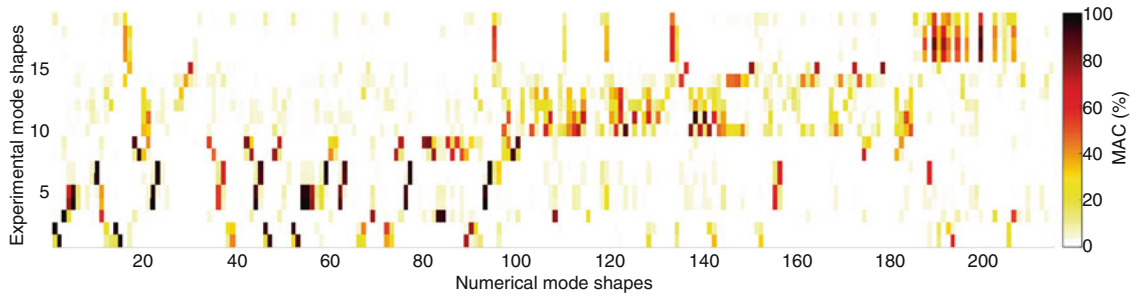

Fig. 13.6 MAC between experimental mode shapes and the first 214 numerical mode shapes

Fig. 13.7 MAC between EMA and preliminary FE model with coarse tuning

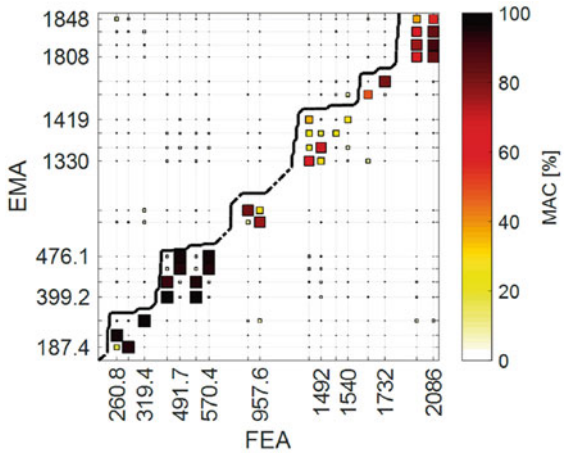

Table 13.2 Experimental and numerical (with and without accelerometer masses) natural frequencies

	Frequency [Hz]		
	Numerical		
Mode description	Without accelerometers	With accelerometers	Experimental
1st bending	268.3–268.3	260.8–260.9	187.4–190.3
1st axial	325.7	319.4	230
2nd bending	491.8–491.8570.6–570.6	476.6–491.7553.4–570.4	399.2–446.3468.2–476.1
1st membrane	692.5–692.5	691.6–691.7	–
1st torsional	705.4	703.8	–
2nd membrane	792.7–792.7	787.4–787.8	–
2nd torsional	952.7	952.3	–
3rd bending	989.7–989.7	957.3–957.6	796.1–797.9
3rd membrane	1472–1472	1469–1470	–
3rd torsional	1472	1471	–
4th torsional	1530	1530	–
4th bending	1535–1535	1490–1492	1330.2–1354.3
In-plane 2-lobe	1568–1568	1539–1540	1392.1–1418.7
In-plane 3-lobe	1738–1738	1660–1732	1607.2–1626.6
4th membrane	1797–1798	1764–1764	–
In-plane 4-lobe	1949–1949	1895–1903	–
5th bending	2217–2217	2017–2086	1808–18131834–1848

high modal density occurs. The lack of correlation for some modes can be attributed to the variability in pretension which not only alters the mode natural frequencies by removing structure axial symmetry but also modal deformation. The model is suitable to describe the dynamics of the bike wheel but is too stiffer since all the frequencies are over estimated. Hence, MU is introduced to obtain a finely tuned FE model.

13.4 Optimisation

For the optimisation process, it is decided to track the first seven experimental mode shapes (first and second bending and axial mode shapes) since the identification and the multiplicity of the other modes at higher frequency is strongly affected by lack of axial symmetry in the prestressed structure. The optimisation is performed by considering the main geometrical and material properties affected by uncertainties. In Table 13.3 the design parameters are listed:

For material properties, the boundaries are imposed for ±50% of the nominal value; on the contrary, a range of two orders of magnitude is supplied to the $t_{mult,rim}$ term, i.e. a multiplier of the rim thickness assumed to be wider since modelisation was based on catalogue data. The pretension N is ranged between 0 N and 3000 N, despite the rim producer maximum spoke tension requirement is 1300 N. In the optimisation algorithm, the first guess is based on nominal values reported in Table 13.1 but reduced of the 25% in order to allow the optimisation tool to start far from sub-optimal condition.

The reliability of the values obtained with the optimisation is checked by running a second process with higher guess (+25%). The aim is to verify that the minimisation of the objective function reached a global minimum.

In Fig. 13.8 the results of the optimisation process are shown.

The process lasts 178 iterations reaching a minimum at 0.183. As can be seen from Fig. 13.8 on the right, the process almost confirmed the Young moduli, while biggest modifications occur to densities. The optimisation process principally redistributes the masses in order to reduce exponential term of MACW2.

MAC in function of EMA and FEA frequencies is plotted in Fig. 13.9.

The identification confirms the effectiveness of the adopted optimisation approach based on mode tracking and frequency weighting. A very good correlation can be remarked for the first and the second bending mode shapes (higher than 93%) as well as for the axial mode shape (97%). A bit smaller MAC correspond to the second bending mode shapes (higher than 94%). Consequently, the MAC correlation is quite high also for modes not tracked in the optimisation: the third bending mode shape is well correlated (at least 90%), while the fourth bending mode ha MAC higher than 51%. Instead, the 2-lobe

Table 13.3 Design parameters for the optimisation with boundaries

Parameter	Lower bound	Starting point	Upper bound	Optimal
E_{rim}, Young Modulus [GPa]	35	52.5	105	68.30
ρ_{rim}, density [kg/m^3]	1350	2025	4050	3589
$t_{mult,rim}$, thickness multiplier [–]	0.1	0.75	10	1.497
E_{spokes}, Young Modulus [GPa]	105	157.5	315	163.3
ρ_{spokes}, density [kg/m^3]	3900	5850	11700	7204
$\varnothing_{spokes}$, diameter [mm]	1	1.5	3	1.617
N, pretension [N]	0	900	3000	529
ρ_{gear}, density [kg/m^3]	3900	5850	11700	6010
ρ_{hub}, density [kg/m^3]	1350	2025	4050	2302

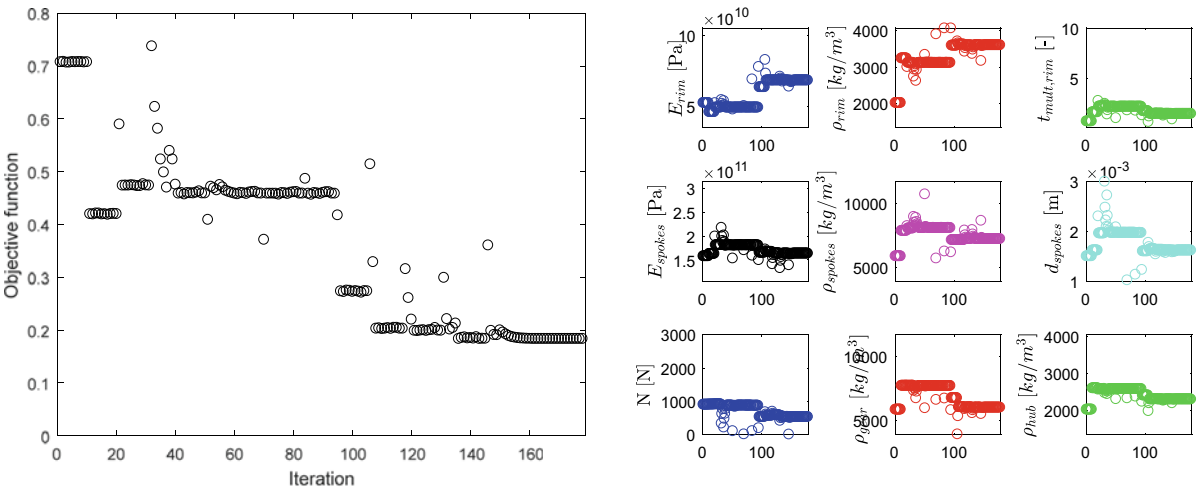

Fig. 13.8 Objective function (left) and parameters (right) trends with respect to the iterations for *fmincon* algorithm

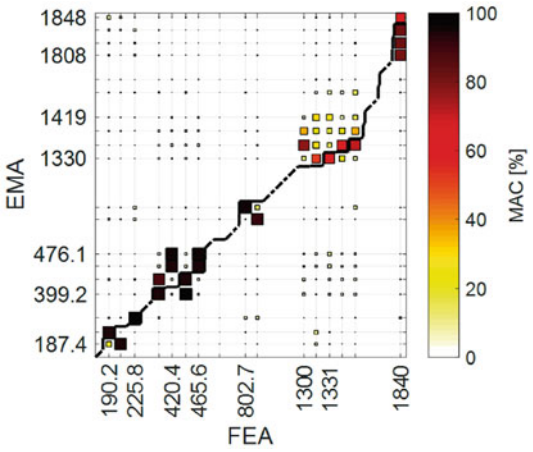

Fig. 13.9 MAC between EMA and preliminary FE model with fine-tuning

Table 13.4 Experimental-numerical comparison of FE finely tuned model

	Frequency [Hz]	
Mode description	Numerical	Experimental
1st bending	190.2–190.3	187.4–190.3
1st axial	225.8	230
2nd bending	403.6–420.4453.6–465.6	399.2–446.3468.2–476.1
3rd bending	802.7.3–803.5	796.1–797.9
4th bending	1306.8–1364.7	1330.2–1354.3
In-plane 2-lobe	–	1392.1–1418.7
In-plane 3-lobe	–	1607.2–1626.6
5th bending	1840	1808–18131834–1848

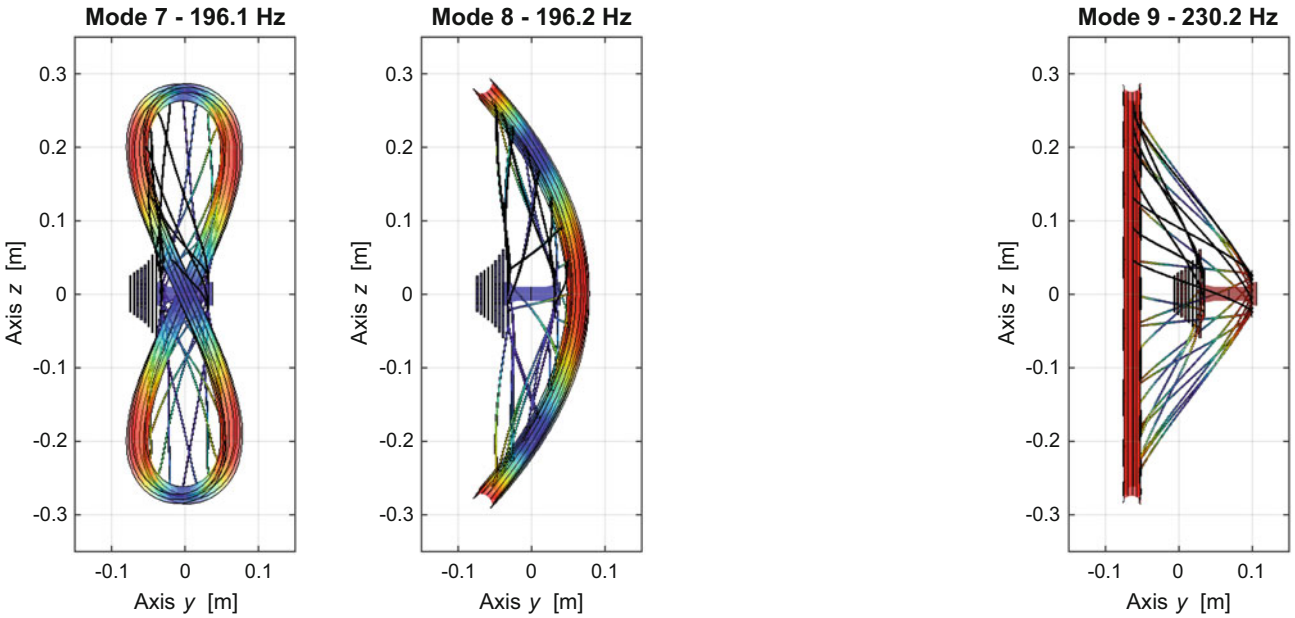

Fig. 13.10 1st bending mode shapes (left and middle), 1st axial mode shape (right)

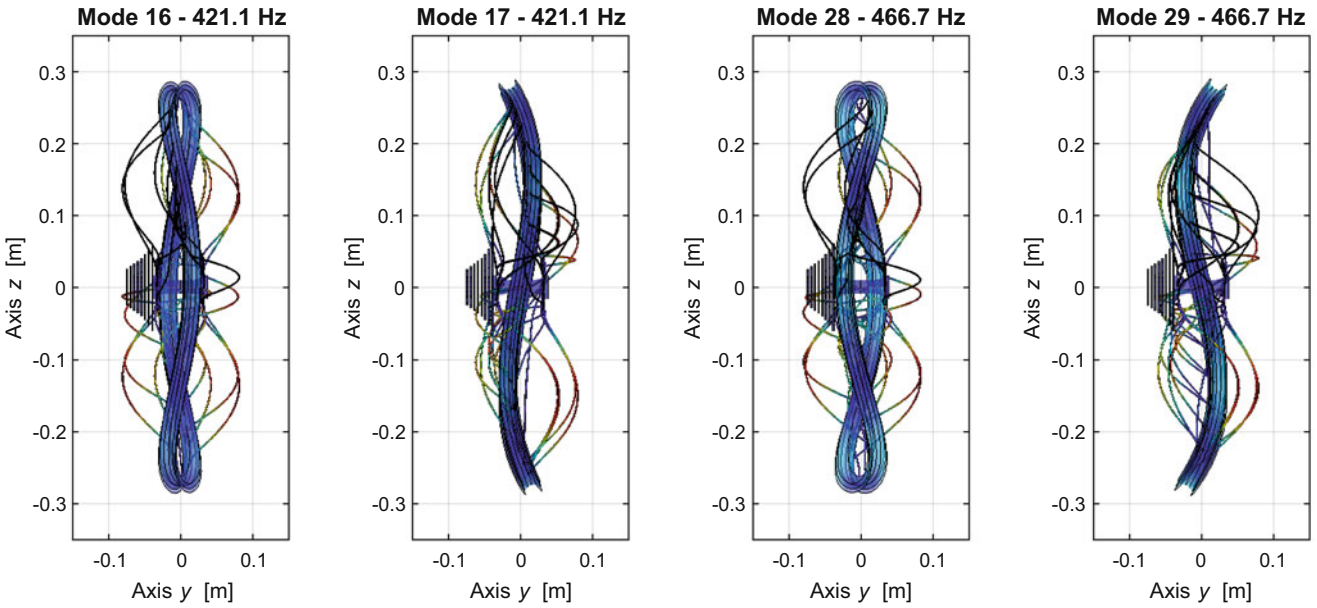

Fig. 13.11 2nd bending mode shapes

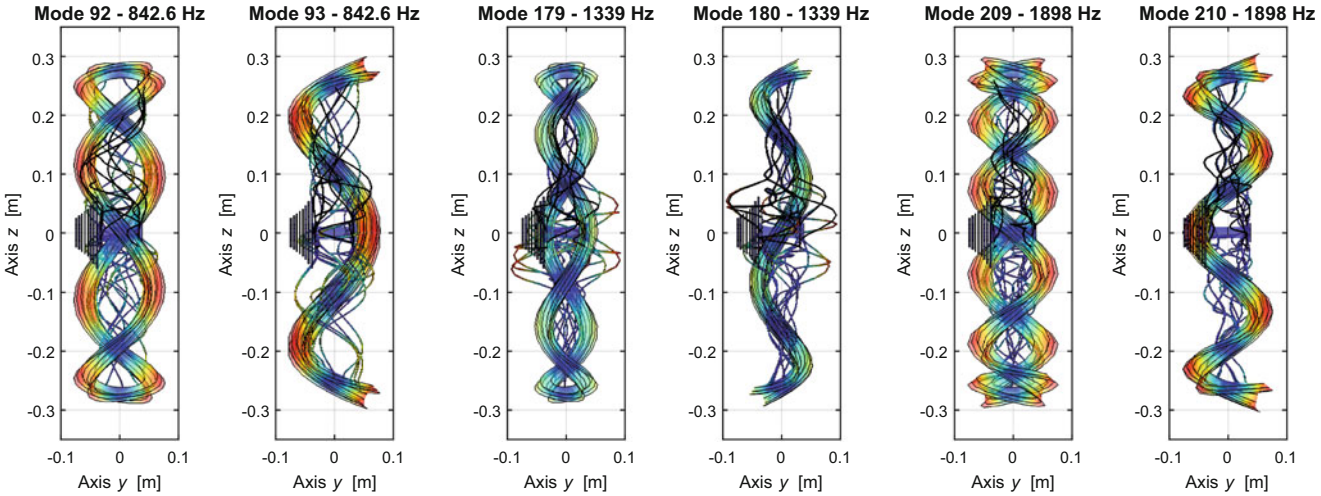

Fig. 13.12 Bending mode shapes from left to right: 3rd modes (1st and 2nd), 4th modes (3rd and 4th), 5th modes (5th and 6th)

in-plane mode shapes own a very poor correlation, almost 10%. The fifth bending mode shapes are well correlated at 80%. The details of the comparison are listed in Table 13.4, considering accelerometer inertial effect.

In the following figures, the numerical mode shapes achieved on the final FE model, without accelerometer adding masses, are shown. In Fig. 13.10 the 1st bending mode shape set and the 1st axial mode shape are shown. In Fig. 13.11 the 2nd bending mode shape set is shown. Finally, in Fig. 13.12 the 3rd, 4th and 5th bending mode shape sets are respectively shown.

13.5 Conclusion

The target of this research activity was the investigation of the modal behaviour of a bike spoke wheel from both experimental and numerical points of view and the application of optimisation algorithm to exploit uncertainties for the model tuning. EMA procedure resulted to be suitable for the identification of the principal structural mode shapes. Good agreement between the primary FE model and experimental result can be highlighted, as for the axial and the bending mode shapes. Between the poles, the identification of in-plane eigenvalues was particularly complex. The model, defined by reference parameters,

results to be stiffer than it was expected. Moreover, high modal density is evidenced both in the FEA and in the EMA. The gap in terms of natural frequencies remarked the presence of a relevant amount of uncertainties. In order to reduce the numerical-experimental mismatching, MU technique is applied, keeping constant the model topology and varying geometrical and material properties. The definition of an objective function to minimise in which overall mass contribution and the difference in terms of eigenvectors and eigenvalues of a mode shape subset was proved to be a robust strategy. Between the parameters, the most relevant variation with respect to the nominal values occurs for inertial properties and spoke thickness.

References

1. Kindt, P., Sas, P., Desmet, W.: Development and validation of a three-dimensional ring-based structural Tyre model. J. Sound Vib. **326**(3–5), 852–869 (2009)
2. Brinkmeier, M., Nackenhorst, U., Petersen, S., Estorff, O.: A finite element approach for the simulation of Tyre rolling noise. J. Sound Vib. **309**, 20–39 (2008)
3. Vella, A.D., Tota, A., Vigliani, A.: On the Road Profile Estimation from Vehicle Dynamics Measurements, SAE Paper 2021-01-1115 (2021)
4. Diaz, C.G., Kindt, P., Middelberg, J., Vercammen, S., Thiry, C., Close, R., Leyssens, J.: Dynamic behaviour of a rolling Tyre: experimental and numerical analyses. J. Sound Vib. **364**, 147–164 (2016)
5. Diaz, G.., Vercammen, S., Middelberg, J., Kindt, P., Thiry, C., Leyssens, J..: Numerical prediction of the dynamic behaviour of rolling tyres. In: Proceedings of ISMA (2012)
6. Doria, A., Taraborrelli, L., Urbani, M.: A modal approach for the study of the transient behavior of motorcycle and scooter Tyres. In: Proceedings of ASME, Buffalo, New York, USA, pp. 29–37. (2014)
7. Dorfi, H.R., Wheeler, R.L., Keum, B.B.: Vibration modes of radial tyres: application to non-rolling and rolling events, SAE Paper 2005-01-2526 (2005)
8. Pinnington, R.J., Briscoe, A.R.: A wave model for a pneumatic Tyre belt. J. Sound Vib. **253**, 941–959 (2002)
9. Kindt, P., Berckmans, D., De Coninck, F., Desmet, W.: Experimental analysis of the structure-borne Tyre/road noise due to road discontinuities. Mech. Syst. Signal Process. **23**, 2557–2574 (2009)
10. Vella, A.D., Vigliani, A., Tota, A., Lisitano, D.: Experimental Ride Comfort Analysis of an Electric Light Vehicle in Urban Scenario, SAE Paper 2020-01-1086 (2020)
11. Bonisoli, E., Marcuccio, G., Venturini, S.: Interference fit estimation through stress-stiffening effect on dynamics. Mech. Syst. Signal Process. **160**, 107919 (2021)
12. Mottershead, J.E., Mares, C., Friswell, M.I., James, S.: Selection and updating of parameters for an aluminium space-frame model. Mech. Syst. Signal Process. **14**(6), 923–944 (2000)
13. Kyprianou, A., Mottershead, J.E.: Uncertain systems: Modelling and updating. In: Proceedings of the 18th ICSV, pp. 995–1002 (2011)
14. Greening, P.D., Lieven, N.A.J.: Identification and updating of loading in frameworks using dynamic measurements. J. Sound Vib. **260**(1), 101–115 (2003)
15. Flores, J.E.R., Viana, F.A.C., Rade, D.A., Steffen Jr., V.: Identification of external forces in mechanical systems by using LifeCycle model and stress-stiffening effect. Mech. Syst. Signal Process. **21**(7), 2900–2917 (2007)
16. Bahra, A.S., Greening, P.D.: Identifying axial load patterns using space frame FEMs and measured vibration data. Mech. Syst. Signal Process. **23**(4), 1282–1297 (2009)
17. Bahra, A.S., Greening, P.D.: Identifying multiple axial load patterns using measured vibration data. J. Sound Vib. **330**(15), 3591–3605 (2011)
18. Allemang, R.J.: A correlation coefficient for modal vector analysis. In: Proceedings of the 1st International Modal Analysis Conference, pp. 110–116. (1982)
19. Allemang, R.J.: The modal assurance criterion–twenty years of use and abuse. Sound Vib. **37**(8), 14–23 (2003)
20. Kranjc, T., Slavič, J., Boltežar, M.: An interface force measurements-based substructure identification and an analysis of the uncertainty propagation. Mech. Syst. Signal Process. **56**, 2–14 (2015)
21. Durand, J.F., Soize, C., Gagliardini, L.: Structural-acoustic modeling of automotive vehicles in presence of uncertainties and experimental identification and validation. J. Acoust. Soc. Am. **124**(3), 1513–1525 (2008)
22. Hinke, L., Dohnal, F., Mace, B.R., Waters, T.P., Ferguson, N.S.: Component mode synthesis as a framework for uncertainty analysis. J. Sound Vib. **324**(1–2), 161–178 (2009)
23. Scigliano, R., Scionti, M., Lardeur, P.: Verification, validation and variability for the vibration study of a car windscreen modeled by finite elements. Finite Elem. Anal. Des. **47**(1), 17–29 (2011)
24. Gallina, A., Lisowski, W., Pichler, L., Stachowski, A., Uhl, T.: Analysis of natural frequency variability of a brake component. Mech. Syst. Signal Process. **32**, 188–199 (2012)
25. Bonisoli E.: LUPOS – LUmped Parameters Open Source FEM code, Tutorial v.2021-09-16
26. Bonisoli, E., Marcuccio, G., Rosso, C.: Crossing and veering phenomena in crank mechanism dynamics. In: Topics in Model Validation and Uncertainty Quantification, vol. 5, pp. 175–187. Springer, New York (2013)
27. Bonisoli, E., Brino, M., Delprete, C.: Numerical-experimental comparison of a parametric test-rig for crossing and veering phenomena. Mech. Syst. Signal Process. **128**, 369–388 (2019)
28. Bonisoli, E., Lisitano, D., Dimauro, L., Peroni, L.: A proposal of dynamic behaviour design based on mode shape tracing: numerical application to a motorbike frame. In: Dynamic Substructures, vol. 4, pp. 149–158. Springer, Cham (2020)
29. https://it.mathworks.com/help/optim/ug/fmincon.html. Available in 2021-10-18

30. https://www.ryde.nl/x-plorer-r. Available in 2021-06-03
31. https://www.purecycles.com/blogs/bicycle-news/156387911-speaking-of-spokes-spoke-patterns. Available in 2021-06-03
32. Bonisoli, E., Delprete, C., Rosso, C.: Proposal of a modal-geometrical-based master nodes selection criterion in modal analysis. Mech. Syst. Signal Process. **23**(3), 606–620 (2009)